Passive Obstacle Aware Control to Follow Desired Velocities

Lukas Huber[1], Trinca Thibaud[1], Jean-Jacques Slotine[2], Aude Billard[1]

***Abstract*— Evaluating and updating the obstacle avoidance velocity for an autonomous robot in real-time ensures robustness against noise and disturbances. A passive damping controller can obtain the desired motion with a torque-controlled robot, which remains compliant and ensures a safe response to external perturbations. Here, we propose a novel approach for designing the passive control policy. Our algorithm complies with obstacle-free zones while transitioning to increased damping near obstacles to ensure collision avoidance. This approach ensures stability across diverse scenarios, effectively mitigating disturbances. Validation on a 7DoF robot arm demonstrates superior collision rejection capabilities compared to the baseline, underlining its practicality for real-world applications. Our obstacle-aware damping controller represents a substantial advancement in secure robot control within complex and uncertain environments.**

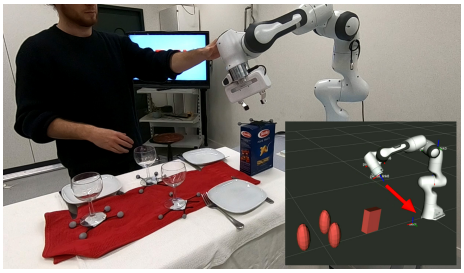

Fig. 1: The proposed passive obstacle-aware controller lets the robot absorb external disturbances while ensuring collision avoidance. While tipping over the closed pasta box on this dinner table setup might be acceptable. Yet, the delicate wine glasses demand careful handling to prevent breakage.

I. Introduction

Robots operating in unstructured, dynamic environments must balance adapting the path to the surroundings and following a desired motion. In human-robot collaboration, they must efficiently complete their tasks while ensuring safe compliance in the presence of potential collisions.

Velocity adjustments based on real-time sensory information are essential in complex and dynamic environments. Achieving this necessitates algorithms that are easily configurable and capable of rapid evaluation. As such, closed-form control laws eliminate the need for frequent replanning. Dynamical Systems (DS) is a valuable framework for representing such desired motion [1] where the behavior of the desired first-order DS is approximated through suitable controllers.

Most widely used robotic systems consist of rigid materials. Consequently, the interaction of these robotic systems with the surroundings leads to abrupt energy transfers, posing the risk of damage to the robot and its environment. However, modern robotic platforms are equipped with force and torque sensing capabilities that enable precise control over the forces exerted by the robot. However, integrating these sensors makes the feedback controller more complex. The robot must achieve its designated position by following a desired velocity profile while remaining compliant with interaction forces. The control problem of balancing position, velocity, and force constraints is addressed by *impedance controllers* [2].

This work was supported by EU ERC grant SAHR.

[1]LASA Laboratory, Swiss Federal School of Technology in Lausanne - EPFL, Switzerland. {lukas.huber;aude.billard}@epfl.ch

[2]Nonlinear Systems Laboratory, Massachusetts Institute of Technology, USA. jjs@mit.edu

Obstacle avoidance is fundamental to motion control, with reactive approaches capable of handling dynamic and intricate environments [1]. The controller should remain compliant in free space while adhering to the desired motion when getting close to the obstacle. Furthermore, when encountering surfaces like fragile glass on a table, the controller must adopt stiffness to prevent a collision, yet it should be compliant when interacting with an operator (Fig. 1).

This work introduces a novel approach incorporating dynamic obstacle avoidance using DS and variable impedance control, enhancing adaptability, reactivity, and safety in robotic movements. It empowers robots to navigate complex environments, proactively avoiding collisions and rejecting disturbances. Our approach is evaluated through an implementation on a 7-degree-of-freedom (7DoF) robot arm, demonstrating robust and safe control in real-world scenarios.

A. Related Work

1) Force Control: Impedance control, a powerful feedback algorithm, effectively applies Cartesian impedance to nonlinear manipulators' end-points [2] . The controller replaces the computationally intensive *inverse kinematics* with the more straightforward *forward kinematics*. Impedance control establishes a dynamic relationship between desired position, velocity, and force, offering a holistic control framework. Initially, impedance controllers employed constant stiffness, but researchers have explored various dynamic control parameter approaches to enhance adaptability in complex environments [3], [4]. However, introducing dynamic parameters into the control framework requires taking special care of the system's stability. Furthermore, admittance control is designed to adapt to external forces while remaining

stable contact [5]. Admittance control can be interpreted as a special type of impedance control.

Passive velocity controllers use a state-dependent velocity, converted into a control force through a damping control law. Since the controllers have variable damping parameters, stability can be guaranteed using storage tanks [6]. However, high compliance often results in decreased motion following. Yet, carefully designing the damping matrix, which increases stiffness in the direction of motion but remains compliant otherwise, results in improved convergence [7]. Combining impedance controllers with admittance controllers can be used to increase accuracy in cooperative control [8]. However, these controllers' adaptations focus on improving movement accuracy rather than actively rejecting disturbances.

Many impedance controllers with time-varying control rely on energy tanks to ensure stability. This is a virtual state, which is filled or emptied depending on the controller command. Limiting the energy tank to a maximum value ensures the system's stability [9]. However, when this limit is reached, the controller is constrained and interferes with the controller's optimal functioning. This can result in the controller not achieving some functionalities, such as collision avoidance. Alternatively, the impedance controller can be constrained by adapting the damping and stiffness and the rate of change based on a Lyapunov function [10].

2) Obstacle Avoidance: In dynamic environments, obstacle avoidance is quickly evaluated to ensure safe robot navigation. Repulsive force fields pointing away from obstacles can create a collision-free motion [11]. However, these artificial potential fields are susceptible to local minima, which led to the introduction of navigation functions. A global function that combines the repulsive force fields while ensuring a global minimum and the goal [12]. Such functions depend on the distribution of the obstacles and are hard to adapt to dynamic environments and high dimensional spaces [13].

Passive controllers can also track the desired motion of the artificial potential field while compensating for Coriolis and centrifugal forces [14]. Nonetheless, these methods lack the guarantee of disturbance repulsion around obstacles, which is addressed by the integration of circular fields, which rotates the robot's path around the obstacles [15]. This allows force-controlled navigation in cluttered environments, yielding convergence for simple obstacles [16]. Conversely, repulsive fields can be combined with elastic, global planning [17] for improved convergence. This allowed adding a repulsive force from the obstacle, ensuring collision avoidance [18]. However, methods based on artificial potential fields are prone to local minima in cluttered environments.

Harmonic potential functions can ensure the absence of local minima in free space [19]. In previous work, we combined harmonic potential functions with the dynamical system framework to obtain reactive, local minima-free motion [1], [20]. It allows for generating a desired velocity based on the robot's position in real time. For implementation on a torque-controlled robot arm, we utilized a passive controller that closely adheres to the desired velocity [7]. However, one of the limitations of the passive controller is its inability to account for the physical surroundings. This makes the robot susceptible to disturbances close to obstacles, potentially leading to collisions. Although DS passive-controlled robots work well in interactive scenarios, they cannot ensure they navigate through an obstacle environment collision-free. For example, they often give in when being pushed toward an obstacle. This work presents a method to address this problem by modifying the passive control law design, making the controller aware of its environment.

B. Contribution

We introduce a passive controller that incorporates into the feedback control loop as visualized in Figure 2. In this work, we make the following contributions:

- A novel obstacle-aware passive controller (Sec. III)
- A passivity guarantee (without storage tank) which applies to general damping controllers (Theorem III.1)
- A collision avoidance analysis which provides insight into the path consistency around obstacles (Sec. IV)
- Implementation and testing on 7DoF robot arm (Sec. V)

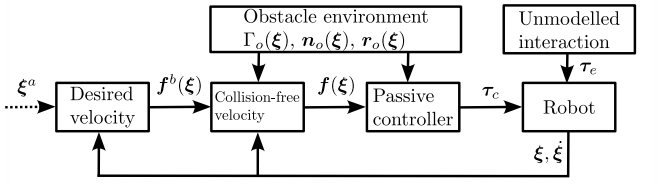

Fig. 2: The desired velocity $\boldsymbol{f}^b(\boldsymbol{\xi})$ can result from a learned velocity field or pointing towards a desired attractor $\boldsymbol{\xi}^a$. The desired velocity is used to evaluate the obstacle avoidance velocity $\boldsymbol{f}(\boldsymbol{\xi})$, fed into the force controller to obtain the control force $\boldsymbol{\tau}_c$. In order to achieve collision avoidance, the distance function $\Gamma_o(\boldsymbol{\xi})$, the normal direction $\boldsymbol{n}_o(\boldsymbol{\xi})$, and the reference direction $\boldsymbol{r}_o(\boldsymbol{\xi})$ are evaluated for each obstacle $o = 1..N^{\text{obs}}$.

II. Preliminaries

Let $\boldsymbol{\xi} \in \mathbb{R}^N$ describe the system's state in an $N \geq 2$ dimensional space, e.g., the robot's joint or Cartesian space positions. The function $\boldsymbol{f}(\boldsymbol{\xi}) : \mathbb{R}^N \rightarrow \mathbb{R}^N$ represents a smoothly defined dynamical system (DS) describing the desired velocity at a given state $\boldsymbol{\xi}$. The first and second-order time derivatives are denoted by one and two dots over the symbol respectively, i.e., $\dot{\boldsymbol{\xi}} = \frac{d}{dt}\boldsymbol{\xi}$ is the systems velocity, and $\ddot{\boldsymbol{\xi}} = \frac{d^2}{dt^2}\boldsymbol{\xi}$ is the acceleration. In general, superscripts are used for variable names, whereas subscripts are used for enumerations.

A. Obstacle Avoidance

Let us assume the base velocity $\boldsymbol{f}^b(\boldsymbol{\xi}) : \mathbb{R}^N \rightarrow \mathbb{R}^N$, which describes the desired, state-dependent motion of the robot. As proposed by [1], [21], an obstacle avoiding velocity $\boldsymbol{f}(\boldsymbol{\xi}) : \mathbb{R}^N \rightarrow \mathbb{R}^N$ can be achieved by a simple matrix multiplication (or modulation) as follows:

$$\begin{aligned} \boldsymbol{f}(\boldsymbol{\xi}) &= \mathbf{E}(\boldsymbol{\xi})\text{diag}\left(\lambda^r, \lambda^e, ..., \lambda^e\right)\mathbf{E}(\boldsymbol{\xi})^{-1}\boldsymbol{f}^b(\boldsymbol{\xi}) \\ \text{with} \quad \mathbf{E}(\boldsymbol{\xi}) &= [\mathbf{r}(\boldsymbol{\xi})\ \mathbf{e}_1(\boldsymbol{\xi})\ ...\ \mathbf{e}_{d-1}(\boldsymbol{\xi})] \end{aligned} \tag{1}$$

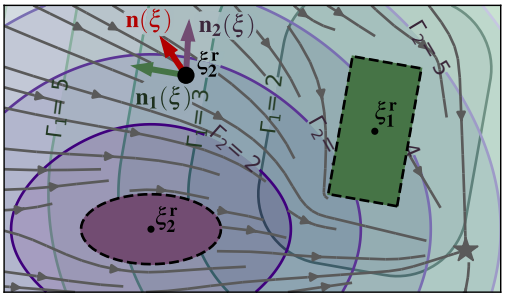

Fig. 3: The Γ-field is defined individually for each of the obstacles. At each position $\boldsymbol{\xi}$, we can evaluate the surface normal $\boldsymbol{n}(\boldsymbol{\xi})$. The velocity $\boldsymbol{f}(\boldsymbol{\xi})$ (gray) avoids collision with the obstacles and converges towards the attractor (star).

where the tangent directions $\mathbf{e}_{(\cdot)} \in \mathbb{R}^N$ are perpendicular to the surface normal $\boldsymbol{n}(\boldsymbol{\xi}) \in \mathbb{R}^N$, see Fig. 3. The reference vector $\mathbf{r}(\boldsymbol{\xi}) = (\boldsymbol{\xi} - \boldsymbol{\xi}^r)/\|\boldsymbol{\xi} - \boldsymbol{\xi}^r\|$ is pointing towards the the reference point $\boldsymbol{\xi}^r \in \mathbb{R}^N$. This construction of the basis matrix is valid for starshaped obstacles, i.e., shapes for which a reference point exists, from which a line in any direction only crosses the surface once [20].

The diagonal values $\lambda_{(\cdot)}$ in (1) are often referred to as eigenvalues since they modify the length of the input velocity in specific directions. The eigenvalue in reference direction $\lambda^r(\boldsymbol{\xi}) \leq 1$, is designed to reduce the velocity towards the obstacle. Conversely, the velocity increases along the tangent direction using $\lambda^e(\boldsymbol{\xi}) \geq 1$. The eigenvalues in reference direction λ^r and tangent direction λ^e are defined as:

$$\lambda^r(\boldsymbol{\xi}) = 1 - 1/\Gamma(\boldsymbol{\xi}), \quad \lambda^e(\boldsymbol{\xi}) = 1 + 1/\Gamma(\boldsymbol{\xi}) \tag{2}$$

with the continuous distance function $\Gamma(\boldsymbol{\xi}) \in \mathbb{R}_{\geq 0}$, which has a value of $\Gamma(\boldsymbol{\xi}) = 1$ on the boundary of an obstacle, and monotonically increases along the normal to the surface of the obstacle (Fig. 3). In this work, we use:

$$\Gamma(\boldsymbol{\xi}) = 1 + \|\boldsymbol{\xi} - \boldsymbol{\xi}^b\|/R^0 \quad \text{with} \quad \boldsymbol{\xi}^b = b(\boldsymbol{\xi} - \boldsymbol{\xi}^r) + \boldsymbol{\xi}^r \tag{3}$$

with $b \in \mathbb{R}_{>0}$, such that $\boldsymbol{\xi}^b \in \mathbb{R}^N$ lies on the surface of the obstacle, and $R^0 \in \mathbb{R})_{>0}$ is the distance scaling, we use $R^0 = 1$.

B. Force Control

1) Rigid Body Dynamics: A force-controlled system is subject to acceleration, inertia, and external disturbances. Its general rigid-body dynamics based on the state $\boldsymbol{\xi}$ are given as

$$\mathcal{M}(\boldsymbol{\xi})\ddot{\boldsymbol{\xi}} + \mathcal{C}(\boldsymbol{\xi}, \dot{\boldsymbol{\xi}})\dot{\boldsymbol{\xi}} + \boldsymbol{g}(\boldsymbol{\xi}) = \boldsymbol{\tau_c} + \boldsymbol{\tau_e} \tag{4}$$

where we have the mass matrix of the robot $\mathcal{M}(\boldsymbol{\xi}) \in \mathbb{R}^{N\times N}$, the Coriolis matrix $\mathcal{C}(\boldsymbol{\xi}, \dot{\boldsymbol{\xi}}) \in \mathbb{R}^N$, the gravity vector $\boldsymbol{g}(\boldsymbol{\xi}) \in \mathbb{R}^N$), the control torque $\boldsymbol{\tau_c} \in \mathbb{R}^N$, and the external torque, also referred as disturbance, $\boldsymbol{\tau_e} \in \mathbb{R}^N$.

2) Damping Controller: Damping control [7] offers a powerful method for computing control forces from a velocity field. This controller provides selective disturbance rejection based on the direction of the desired motion. Typically, the controller is configured with high damping along the direction of motion, ensuring rapid convergence of the robot's velocity to the desired value and achieving excellent tracking performance. In contrast, the controller exhibits high compliance in the direction perpendicular to the motion, enabling flexible behavior and greater resistance to external forces. The passive control force is evaluated as follows:

$$\boldsymbol{\tau_c} = \boldsymbol{g}(\boldsymbol{\xi}) + \mathcal{D}(\boldsymbol{\xi})\left(\boldsymbol{f}(\boldsymbol{\xi}) - \dot{\boldsymbol{\xi}}\right) \tag{5}$$

This control law embeds a gravity compensation term $\boldsymbol{g}(\boldsymbol{\xi}) \in \mathbb{R}^N$ and a positive-definite damping term, which dampens the difference between the desired velocity $\boldsymbol{f}(\boldsymbol{\xi})$ and the actual velocity $\dot{\boldsymbol{\xi}}$. The positive definite damping matrix $\mathcal{D}(\boldsymbol{\xi}) \in \mathbb{R}^{N\times N}$ is given as:

$$\mathcal{D}(\boldsymbol{\xi}) = \mathcal{Q}(\boldsymbol{\xi})\mathcal{S}(\boldsymbol{\xi})\mathcal{Q}(\boldsymbol{\xi})^{-1} \tag{6}$$

where $\mathcal{Q}(\boldsymbol{\xi}) = [\boldsymbol{q}_1\,,\ \boldsymbol{q}_2\ ,\ \ldots\,,\ \boldsymbol{q}_N]$ is an orthonormal basis matrix, of which the first vector is pointing in the desired direction of motion

$$\boldsymbol{q}_1(\boldsymbol{\xi}) = \boldsymbol{q}_1^f(\boldsymbol{\xi}) = \boldsymbol{f}(\boldsymbol{\xi})/\|\boldsymbol{f}(\boldsymbol{\xi})\| \tag{7}$$

The diagonal matrix $\mathcal{S}(\boldsymbol{\xi}) \in \mathbb{R}^{N\times N}$ consists of damping factors $s_i \in \mathbb{R}_{>0}$ in the corresponding direction $i = 1..N$. This design allows the separate design of the damping in the direction of motion and perpendicular to the motion. Increased consistency with the desired velocity is achieved by using a high value for the first damping factor. Conversely, the damping in the remaining directions is set lower to allow compliance perpendicular to the motion, i.e., $s_i/s_1 \ll 1,\ i = 2..N$.

III. Obstacle Aware Passivity

We propose a novel controller, which ensures passivity as defined in (5) but adapts the damping matrix given in (6) based on the desired velocity $\dot{\boldsymbol{\xi}}$ and obstacles in the surrounding. Far away from obstacles, the system is designed to follow the initial velocity, but approaching the obstacle increases the damping, decreasing the chance of a collision.

Hence, the damping matrix $\mathcal{D}(\boldsymbol{\xi}) \in \mathbb{R}^{N\times N}$ smoothly changes from being aligned with the direction of the velocity, as used in [7], to be aligned with the averaged normal of the obstacles. The desired damping matrix transitions between velocity preserving and collision avoidance using a smoothly defined linear combination:

$$\mathcal{D}(\boldsymbol{\xi}) = (1 - w(\boldsymbol{\xi}))\,\mathcal{D}^f(\boldsymbol{\xi}) + w(\boldsymbol{\xi})\mathcal{D}^o(\boldsymbol{\xi}) \tag{8}$$

The damping matrix is made up of two components: the velocity damping. $\mathcal{D}^f \in \mathbb{R}^{N\times N}$ which prioritizes following the desired velocity similar to [7], and the obstacle damping $\mathcal{D}^o \in \mathbb{R}^{N\times N}$ which is designed to reject disturbances towards obstacles. The two damping matrices are positive definite and are smoothly summed using the danger weight $w(\boldsymbol{\xi}) \in [0, 1]$. Far away from obstacles the weight reaches $w(\boldsymbol{\xi}) = 0$, whereas $w(\boldsymbol{\xi}) = 1$ when approaching a boundary:

$$w(\boldsymbol{\xi}) = \max\left(0, \frac{\Gamma^{\text{crit}} - \Gamma(\boldsymbol{\xi})}{\Gamma^{\text{crit}} - 1}\right)\|\boldsymbol{n}(\boldsymbol{\xi})\| \quad \text{with} \quad \Gamma(\boldsymbol{\xi}) = \min_{o=1..N^{\text{obs}}} \Gamma_o(\boldsymbol{\xi}) \tag{9}$$

The critical distance defines the distance where the system increases the damping towards the obstacle. $\mathcal{D}^f(\boldsymbol{\xi})$ and $\mathcal{D}^{\text{obs}}(\boldsymbol{\xi})$ follow design given in (6) and are positive definite matrices, thus $\mathcal{D}(\boldsymbol{\xi})$ is positive definite, too.

A. Damping for Collision Repulsion

1) Normal Direction: The damping matrix $\mathcal{D}^{\text{o}}(\boldsymbol{\xi})$ rejects velocities in the direction of the obstacles. To allow this, we introduce an averaged normal direction:

$$\boldsymbol{n}(\boldsymbol{\xi}) = \sum_{o=1}^{N^{\text{o}}} \boldsymbol{n_o}(\boldsymbol{\xi}) \frac{1/(\Gamma_o(\boldsymbol{\xi})-1)}{\sum_{p=1}^{N^{\text{o}}} 1/(\Gamma_p(\boldsymbol{\xi})-1)} \tag{10}$$

where the unit normals $\boldsymbol{n_o}(\boldsymbol{\xi})$ pointing away from the obstacle $o = 1, .., N^{\text{o}}$ and are perpendicular to the surface, see Figure 3.

The averaged normal $\boldsymbol{n}(\boldsymbol{\xi})$ is a weighted linear combination of the obstacles' normals, giving more importance to closer obstacles. Additionally, the averaged normal converges to an obstacle normal as we converge towards it, i.e., $\lim_{\Gamma_o(\boldsymbol{\xi})\to 1} \boldsymbol{n}(\boldsymbol{\xi}) = \boldsymbol{n}_o(\boldsymbol{\xi})$. Note that the averaged normal is a zero-vector when two obstacles oppose each other.

2) Decomposition Matrix: The decomposition matrix $\mathcal{Q}^{\text{o}}(\boldsymbol{\xi})$ has its first vector aligned with the normal to the obstacle:

$$\boldsymbol{q}_1^{\text{o}}(\boldsymbol{\xi}) = \boldsymbol{n}(\boldsymbol{\xi})/\|\boldsymbol{n}(\boldsymbol{\xi})\| \quad \forall\, \boldsymbol{\xi} : \|\boldsymbol{n}(\boldsymbol{\xi})\| > 0 \tag{11}$$

In the case that $\|\boldsymbol{n}(\boldsymbol{\xi})\| = 0$, the danger weight $w(\boldsymbol{\xi})$ from (9) reaches 0. Hence, the obstacle-aware damping in (8) has no effect and is not evaluated.

The second vector is set to be aligned with the desired velocity as much as possible, allowing increased velocity following (Fig. 3). However, it has to remain orthonormal to $\boldsymbol{q}_1^{\text{o}}$

$$\boldsymbol{q}_2^{\text{o}} = \frac{\hat{\boldsymbol{q}}_2^{\text{o}}}{\|\hat{\boldsymbol{q}}_2^{\text{o}}\|} \quad \hat{\boldsymbol{q}}_2^{\text{o}} = \boldsymbol{q}_1^f - \boldsymbol{q}_1^{\text{o}} p \quad \forall\, \boldsymbol{\xi} : |p| < 1 \tag{12}$$

where velocity unit vector $\boldsymbol{q}_1^f$ is defined in (7), and the object weight is evaluated as $p = \left\langle \boldsymbol{q}_1^{\text{o}},\, \boldsymbol{q}_1^f \right\rangle$. For the case that $|p| = 1$, the second basis $\boldsymbol{q}_2^{\text{o}}$ is set to be any orthonormal vector. The remaining vectors $\boldsymbol{q}_d^{\text{o}}, d = 3, .., N$ are constructed to form an orthonormal basis to the first two.

3) Damping Values: We define the values of the diagonal matrix $\mathcal{S}^{\text{o}}(\boldsymbol{\xi})$ as

$$\mathcal{S}_d^{\text{o}}(\boldsymbol{\xi}) = \begin{cases} s^{\text{o}} & d = 1 \\ |p| s^c + (1-|p|) s^f & d = 2 \\ s^c & d = 3..N \end{cases} \tag{13}$$

where the damping along the nominal direction $s^f \in \mathbb{R}_{>0}$, obstacle-damping $s^{\text{o}} \in \mathbb{R}_{>0}$, and the compliant-damping $s^c \in \mathbb{R}_{>0}$ are user-defined parameters which determine the behavior of the passive-controller. The first entry of $\boldsymbol{S}^{\text{o}}$ dictates the damping towards the obstacle, and the second entry the desired velocity following. Note how the second value approaches the compliant damping, as normal and velocity become parallel.

To ensure continuity across time of the control force as defined in (5), the values of the diagonal damping matrix $\mathcal{S}^{\text{o}}(\boldsymbol{\xi})$ in the tangent directions are equal when the normal aligns with the velocity, i.e.:

$$\lim_{|p|\to 1} \mathcal{S}_d = \mathcal{S}_e, \quad d > 2..N,\, e > 2..N \tag{14}$$

Hence, the choice of orthonormal vectors $\boldsymbol{q}_d^{\text{o}}, d > 2..N$ does not influence the control force as long as the matrix Q^{d} has full rank.

4) Damping Only Towards Obstacle: In the presence of an obstacle, the disturbances should be damped strongly when the agent is pushed against the obstacle. Conversely, the system can remain compliant if the motion is away from the obstacle. This is achieved by setting updating the first damping value $\mathcal{S}_1^{\text{o}}$ if the robot is moving away from the surface:

$$\mathcal{S}_1^{\text{o}}(\boldsymbol{\xi}) = \begin{cases} s^{\text{o}} & \text{if } \left(\boldsymbol{f}(\boldsymbol{\xi}) - \dot{\boldsymbol{\xi}}\right)^T \boldsymbol{n}(\boldsymbol{\xi}) > 0 \\ s^{\text{c}} & \text{otherwise} \end{cases} \tag{15}$$

Since $\boldsymbol{q}_1^o(\boldsymbol{\xi})$ given in (11) is pointing along the obstacle normal $\boldsymbol{n}(\boldsymbol{\xi})$, the first obstacle damping value $\mathcal{S}_1^{\text{o}}(\boldsymbol{\xi})$ does not have any effect on the control force $\boldsymbol{\tau}^c$ given in (5) when $\left(\boldsymbol{f}(\boldsymbol{\xi}) - \dot{\boldsymbol{\xi}}\right)^T \boldsymbol{n}(\boldsymbol{\xi}) = 0$. Hence, the damping value can be discontinuous across time, but the resulting control force remains continuous.

B. Damping for Velocity Preservation

The decomposition matrix $\mathcal{Q}^f$ is an orthonormal basis with the first vector being parallel to the desired velocity $\boldsymbol{f}(\boldsymbol{\xi})$. Hence, the values of the diagonal matrix $\mathcal{S}^f$ are high in the direction of the desired velocity (first component) but more compliant in the remaining directions. Moreover, the damping is set to ensure that when passing a narrow passage between two obstacles, where the normal vector cancels $\boldsymbol{n}(\boldsymbol{\xi}) \approx \boldsymbol{0}$, with additionally a low distance value $\Gamma(\boldsymbol{\xi}) \approx 1$, the damping perpendicular to the velocity direction is high. We set:

$$\begin{aligned} \mathcal{S}_d^f &= w^p s^{\text{o}} + \begin{cases} (1-w^p) s^f & d = 1 \\ (1-w^p) s^s & d = 2..N \end{cases} \\ \text{with} \quad & w^p = \min\left(1, \|\boldsymbol{n}(\boldsymbol{\xi})\|^2 + \Delta\Gamma^2\right) \\ \text{and} \quad & \Delta\Gamma = \max\left(\frac{\Gamma^{\text{crit}} - \Gamma(\boldsymbol{\xi})}{\Gamma^{\text{crit}} - 1}, 0\right) \end{aligned} \tag{16}$$

C. Cluttered Environments

In a cluttered environment, the normal vectors of the individual obstacles can be opposing. And hence using (10) and (9), we get:

$$\|\boldsymbol{n}(\boldsymbol{\xi})\| \to 0 \quad \text{and} \quad \lim_{\Gamma(\boldsymbol{\xi})\to 1} w(\boldsymbol{\xi}) = 0 \tag{17}$$

Additionally using (8) and (16) we obtain:

$$\lim_{\Gamma\to 1, \|n\|\to 0} \mathcal{D}(\boldsymbol{\xi}) = \mathcal{D}^S(\boldsymbol{\xi}) + 0 = \mathcal{I} s^o \tag{18}$$

Hence, there is high damping in all directions to reject disturbances towards potential obstacles and ensure a collision-free motion even in cluttered environments.

D. Passivity Analysis

The stability analysis of the system gives information about the stability region of the proposed controller. We analyze passivity by observing the evolution of the kinetic energy of the system, given as:

$$W(\boldsymbol{\xi}, \dot{\boldsymbol{\xi}}) = \frac{1}{2}\dot{\boldsymbol{\xi}}^T \mathcal{M}(\boldsymbol{\xi})\dot{\boldsymbol{\xi}} \tag{19}$$

Lemma III.1. *Let us assume a robotic system as described in* (4) *is controlled using* (5) *using the damping matrix* $\mathcal{D}(\boldsymbol{\xi})$ *given in* (8) *with damping values* $s_d = 1, d = 1..N$. *The system is passive with respect to the input-output pair* $\boldsymbol{\xi}_e$, $\dot{\boldsymbol{\xi}}$ *when exceeding the desired velocity* $\boldsymbol{f}(\boldsymbol{\xi})$ *, i.e.,* $\dot{W} \leq \dot{\boldsymbol{\xi}}^T \boldsymbol{\tau}^e$, $\forall \boldsymbol{\xi} \in \mathbb{R}^N : \|\dot{\boldsymbol{\xi}}\| \geq \|\boldsymbol{f}(\boldsymbol{\xi})\|$ *and the storage function being the kinetic energy* $W \in \mathbb{R}_{>0}$ *given in* (19)

Proof: The time derivative of storage function W can be evaluated as:

$$\begin{aligned}\dot{W}(\boldsymbol{\xi}, \dot{\boldsymbol{\xi}}) &= \dot{\boldsymbol{\xi}}^T \mathcal{M}(\boldsymbol{\xi})\ddot{\boldsymbol{\xi}} + \frac{1}{2}\dot{\boldsymbol{\xi}}^T \dot{\mathcal{M}}(\boldsymbol{\xi})\dot{\boldsymbol{\xi}} \\ &= \frac{1}{2}\dot{\boldsymbol{\xi}}^T \left(\dot{\mathcal{M}}(\boldsymbol{\xi}) - 2\mathcal{C}(\boldsymbol{\xi})\right)\dot{\boldsymbol{\xi}} - \dot{\boldsymbol{\xi}}^T \mathcal{D}(\boldsymbol{\xi})\left(\dot{\boldsymbol{\xi}} - \boldsymbol{f}(\boldsymbol{\xi})\right) + \dot{\boldsymbol{\xi}}^T \boldsymbol{\tau}^e \\ &= -\dot{\boldsymbol{\xi}}^T \mathcal{D}(\boldsymbol{\xi})\left(\dot{\boldsymbol{\xi}} - \mathbf{f}(\boldsymbol{\xi})\right) + \dot{\boldsymbol{\xi}}^T \boldsymbol{\tau}^e \end{aligned} \tag{20}$$

where the second order dynamics $\ddot{\boldsymbol{\xi}}$ are evaluated according to the rigid body dynamics defined in (4). Furthermore, $\dot{\mathcal{M}} - 2\mathcal{C}$ is skew-symmetric for any physical system; hence, the corresponding summand is zero.

Let us investigate the region where the passivity holds. Since in the Lemma, we assumed all damping values to be equal to one, we have:

$$\mathcal{D}(\boldsymbol{\xi}) = \mathcal{Q}(\boldsymbol{\xi})\mathcal{S}(\boldsymbol{\xi})\mathcal{Q}(\boldsymbol{\xi})^{-1} = \mathcal{Q}(\boldsymbol{\xi})\mathcal{I}\mathcal{Q}(\boldsymbol{\xi})^{-1} = \mathcal{I} \tag{21}$$

where $\mathcal{I} \in \mathbb{R}^{N \times N}$ is the identity matrix.

It follows that the system is passive with respect to the input, the external force τ^e, and the output, the velocity $\dot{\boldsymbol{\xi}}$, if:

$$\dot{\boldsymbol{\xi}}^T \mathcal{D}(\boldsymbol{\xi})\left(\dot{\boldsymbol{\xi}} - \boldsymbol{f}(\boldsymbol{\xi})\right) = \dot{\boldsymbol{\xi}}^T \Delta\boldsymbol{f} \geq 0\,, \quad \Delta\boldsymbol{f} = \dot{\boldsymbol{\xi}} - \boldsymbol{f}(\boldsymbol{\xi}) \tag{22}$$

On the border of this region, the two vectors $\Delta\boldsymbol{f}$ and $\dot{\boldsymbol{\xi}}$ are orthogonal. Hence, using Thale's theorem, this region can be interpreted as a circle in velocity-space with radius $\|\boldsymbol{f}(\boldsymbol{\xi})\|/2$ and center $\boldsymbol{f}(\boldsymbol{\xi})/2$, see Figure 4.

Moreover, the system is passive as long as the observed velocity $\dot{\boldsymbol{\xi}}$ is outside the circular-red region, which is a subset of the region where the magnitude of the observed velocity is smaller than the desired velocity $\boldsymbol{f}(\boldsymbol{\xi})$, i.e.,

$$\dot{W}(\boldsymbol{\xi}, \dot{\boldsymbol{\xi}}) \leq \dot{\boldsymbol{\xi}}^T \boldsymbol{\tau}^e \quad \forall \boldsymbol{\xi} : \|\dot{\boldsymbol{\xi}}\| \geq \|\boldsymbol{f}(\boldsymbol{\xi})\| \tag{23}$$

As in the orange region, the system is not passive; the storage function W could increase, and hence, the velocity $\dot{\boldsymbol{\xi}}$ increases non-passively. This behavior is not unexpected, as the controller is designed to approach the desired dynamics $\boldsymbol{f}(\boldsymbol{\xi})$. Hence, as long as the desired velocity is not reached, the kinetic energy increases even with no force input $\boldsymbol{\tau}^e$. However, as soon as the system velocity $\dot{\boldsymbol{\xi}}$ exceeds the desired velocity $\boldsymbol{f}(\boldsymbol{\xi})$, the system behaves passively. We can use this to ensure the stability of the system:

Theorem III.1. *Let* $\boldsymbol{f}(\boldsymbol{\xi})$ *is the desired velocity with bounded magnitude, i.e.,* $\|\boldsymbol{f}(\boldsymbol{\xi})\| < v^{\max}, \forall \boldsymbol{\xi} \in \mathbb{R}^N$. *The closed loop system* (4) *using the controller from* (5) *and the damping matrix* $\mathcal{D}(\boldsymbol{\xi})$ *given in* (8) *is bounded-input, bounded-output (BIBO) stable with respect to the input disturbance force* $\boldsymbol{\tau}^e$, *and output the velocity* $\dot{\boldsymbol{\xi}}$ *for all times* $T = 0, .., \infty$.

Proof:

To ensure BIBO stability, let us analyze the integral of the impulse of the response for the external force $\boldsymbol{\tau}^e$:

$$\begin{aligned}\int_0^T \left\|\dot{\boldsymbol{\xi}}\right\| \, dt &= \int_{t \notin \mathcal{T}_n} \left\|\dot{\boldsymbol{\xi}}\right\| \, dt + \int_{t \in \mathcal{T}_n} \left\|\dot{\boldsymbol{\xi}}\right\| \, dt \\ &\leq K_p + v^{\max} T_n \end{aligned} \tag{24}$$

where $\mathcal{T}_n$ denotes the set of time instances where the system is not shown to be passive (Fig. 4), specifically $\|\dot{\boldsymbol{\xi}}\| \leq \|\boldsymbol{f}(\boldsymbol{\xi})\|$, and $T_n \in \mathbb{R}_{\geq 0}$ is the total duration which the system spends in this region. Additionally, from passivity in the inner region, the system is bounded by a constant $K_p \in \mathbb{R}_{\geq 0}$. Hence, the impulse response is bounded, and the system is BIBO stable.

However, from (8), we know that a general damping matrix $\mathcal{S}(\boldsymbol{\xi})$ can have non-uniform diagonal values. This is analyzed by introducing the coordinate transfers:

$$\bar{\boldsymbol{v}} = \sqrt{\mathcal{S}(\boldsymbol{\xi})}\mathcal{Q}(\boldsymbol{\xi})^{-1}\dot{\boldsymbol{\xi}} \;\text{ and }\; \bar{\Delta\boldsymbol{f}} = \sqrt{\mathcal{S}(\boldsymbol{\xi})}\mathcal{Q}(\boldsymbol{\xi})^{-1}\Delta\boldsymbol{f} \tag{25}$$

where the square root of the diagonal matrix $\mathcal{S}(\boldsymbol{\xi})$ is taken element-wise. The transfer is then used to rewrite (22) as:

$$\dot{\boldsymbol{\xi}}^T \mathcal{D}(\boldsymbol{\xi})\Delta\boldsymbol{f} = \dot{\boldsymbol{\xi}}^T \mathcal{Q}(\boldsymbol{\xi})\mathcal{S}(\boldsymbol{\xi})\mathcal{Q}(\boldsymbol{\xi})^{-1}\Delta\boldsymbol{f} = \bar{\boldsymbol{v}}^T \bar{\Delta\boldsymbol{f}} \tag{26}$$

Hence, the BIBO analysis of (24) applied to the transformed system results as:

$$\begin{aligned}\int_0^T \|\bar{\boldsymbol{v}}\| \, dt &= \int_{t \notin \bar{\mathcal{T}}_n} \|\bar{\boldsymbol{v}}\| \, dt + \int_{t \in \bar{\mathcal{T}}_n} \|\bar{\boldsymbol{v}}\| \, dt \\ &< K_p + v^{\max} \bar{T}_n \max\left(\text{eig}(\mathcal{D})\right) / \min\left(\text{eig}(\mathcal{D})\right) \end{aligned} \tag{27}$$

where $\bar{\mathcal{T}}_n$ denotes the region where the transformed system $\bar{\boldsymbol{v}}$ is not shown to be passive, i.e. $\|\bar{\boldsymbol{v}}\| \leq \|\bar{\Delta\boldsymbol{f}}\|$, and $\bar{T}_n \in$

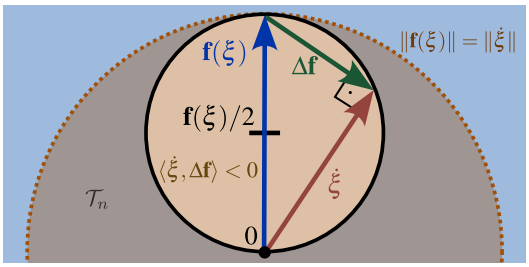

Fig. 4: Analyzing the system in velocity-space yields that the system is passive if it has a velocity $\dot{\boldsymbol{\xi}}$ larger than the desired velocity $\boldsymbol{f}(\boldsymbol{\xi})$, i.e., outside the dashed circle. However, the system can be non-passive for small velocities when $\left\langle \dot{\boldsymbol{\xi}}, \Delta\boldsymbol{f} \right\rangle < 0$ (yellow circle).

$\mathbb{R}_{\geq 0}$ the corresponding time. Additionally, $\min(\text{eig}(\mathcal{D}))$ and $\max(\text{eig}(\mathcal{D}))$ are the smallest and largest eigenvalue of the damping matrix $\mathcal{D}$ respectively.

Hence, since the transformed system with velocity $\bar{\boldsymbol{v}}$ is BIBO stable, the original system with velocity $\dot{\boldsymbol{\xi}}$ is BIBO stable, too, as long as it is a continuous, finite transform.

For an orthogonal decomposition matrix $\mathcal{Q}(\boldsymbol{\xi})$, the region of non-passivity is an ellipse where the direction of the axes points along column vectors of $\mathcal{Q}(\boldsymbol{\xi})$, and the corresponding axes lengths are the diagonal elements of $\|\mathbf{f}(\boldsymbol{\xi})^T\sqrt{\mathcal{S}(\boldsymbol{\xi})}\|/2\sqrt{\mathcal{S}(\boldsymbol{\xi})}^{(-1)}$. If the ratio of the first damping value to the other axis $i \geq 2$ is large, i.e., $s_1/s_i \gg 1$, it can lead to non-passivity even though the velocity $\dot{\boldsymbol{\xi}}$ is already larger (but not pointing in the correct direction) than the desired velocity. However, the non-passive region is still bounded. This proof holds for any basis $\mathcal{Q}$ which is not singular. However, the controller must be carefully chosen to ensure that the speed up is limited when the basis is close to singular, for example, by limiting the relative difference of the stretching vectors. Furthermore, as stable behavior is ensured for a general shape of a damping matrix $\mathcal{D}(\boldsymbol{\xi})$, the global stability proof extends to any positive definite damping matrix matrices.

Since the damping matrix $\mathcal{D}(\boldsymbol{\xi})$ changes dynamically, a change in the environment can move the system outside of the passive region. However, a finite maximum velocity always exists, at which the system is ensured to be passive.

IV. Collision Avoidance

The principal goal of the controller introduced in the previous section is its ability to ensure collision avoidance in the presence of external disturbances. However, the control force $\boldsymbol{\tau}^c$ proposed in (5) does not explicitly consider external forces. Yet, it is designed to correct the agent's velocity $\dot{\boldsymbol{\xi}}$ if it deviates from the desired velocity $\ddot{\boldsymbol{\xi}}$.[1]

Since interaction with the environment results in a force on the system, often over a short period $\Delta t \ll 1$. Hence, we can define the velocity after impact $\boldsymbol{v}^I$ as:

$$\boldsymbol{v}^I \approx \int_{t^I}^{t^I+\Delta t} \ddot{\boldsymbol{\xi}} dt \approx \int_{t^I}^{t^I+\Delta t} \mathcal{M}^{-1}(\boldsymbol{\xi})\boldsymbol{\tau}_e \, dt \qquad (28)$$

using the controller from (4), and under absence of the control force $\boldsymbol{\tau}_c$ during this short timeframe. Additionally, $\{\boldsymbol{\xi}\}_{t^I}$ is the velocity before the impact.

Furthermore, let us consider a desired velocity $\boldsymbol{f}(\boldsymbol{\xi})$, which is a constant, collision-free vector field parallel to the surface of a flat obstacle surface (see Fig. 5):

$$\langle \boldsymbol{f}(\boldsymbol{\xi}), \boldsymbol{n}(\boldsymbol{\xi})\rangle = 0 \qquad \boldsymbol{f}(\boldsymbol{\xi}) = \text{const.}\,,\ \boldsymbol{n}(\boldsymbol{\xi}) = \text{const.} \quad (29)$$

where $\boldsymbol{n}(\boldsymbol{\xi})$ is the surface's normal vector, and the agent moves in a straight line, hence we can neglect the Coriolis effect. For disturbances in such environments, we show that our approach can ensure the impenetrability of the obstacle up to an upper bound on the magnitude of the disturbance:

[1]Note that for a discrete-time (digital) controller, this results in a delay.

Lemma IV.1. *Consider a point-mass agent with mass $m \in \mathbb{R}_{>0}$, whose motion evolves according to the rigid body dynamics given in* (4) *controlled by* (5)*, with constant damping matrix $\mathcal{D}$ from* (8)*. The agent tracks a constant reference velocity* f*, whose vector field moves parallel to a flat obstacle as given in* (29)*. Any motion path initiated in free space will remain collision-free for all times, i.e., $\Gamma(\{\boldsymbol{\xi}_t\}) \geq 1$ with $t \geq 0$ if the impact velocity v^I as given in* (28) *at time $t = 0$ is limited by $\|\boldsymbol{v}^I\| < s^{\text{f}}\|\boldsymbol{\xi} - \boldsymbol{\xi}^b\|/m$, with respect to the closest surface point $\boldsymbol{\xi}^b \in \mathbb{R}^N$.*

Proof: According to the Bony-Bezis theorem [22], the trajectories are collision-free if there is zero velocity towards the obstacle on the surface, i.e.,

$$\left|\boldsymbol{n}(\boldsymbol{\xi})^T\{\dot{\boldsymbol{\xi}}\}_t\right| = 0 \quad \forall \Gamma(\boldsymbol{\xi}) = 1 \qquad (30)$$

We want to find the time when the agent stops moving towards the obstacle, enabling us to evaluate the distance traveled as a function of the velocity after disturbance $\boldsymbol{v}^I$. Let us assume without loss of generality that the disturbance occurs at time $t = 0$. Hence, the velocity at time T can be computed as:

$$\begin{aligned}\{\dot{\boldsymbol{\xi}}\}_T &= \int_0^T \ddot{\boldsymbol{\xi}}\, dt = \int_0^T \mathcal{M}^{-1}\mathcal{D}\left(\dot{\boldsymbol{\xi}} - \boldsymbol{f}(\boldsymbol{\xi})\right) dt \\ &= \mathcal{M}^{-1}\int \left((1-w)\mathcal{D}^f + w\mathcal{D}^o\right)\left(\dot{\boldsymbol{\xi}} - \boldsymbol{f}(\boldsymbol{\xi})\right) dt\end{aligned} \qquad (31)$$

Furthermore, since the vector field, $\boldsymbol{f}(\boldsymbol{\xi})$ is constant and the obstacle's surface does not have any curvature, it follows from (8) that the damping matrices $\mathcal{D}^o$ and $\mathcal{D}^f$ are constant. Moreover, by design of the damping matrices, from (11) it follow that $\mathcal{D}^o(\boldsymbol{\xi})\boldsymbol{n}(\boldsymbol{\xi}) = s^o\boldsymbol{n}(\boldsymbol{\xi})$, and from (7) that $\mathcal{D}^f(\boldsymbol{\xi})\boldsymbol{n}(\boldsymbol{\xi}) = s^f\boldsymbol{n}(\boldsymbol{\xi})$.

From (30) follows that it is sufficient to observe the normal component of the vectors only. Thus, in the rest of this paragraph, the components along the normal are denoted by scalar values, e.g. $\dot{\xi} = \left\langle \dot{\boldsymbol{\xi}}, \boldsymbol{n}(\boldsymbol{\xi})\right\rangle \boldsymbol{n}(\boldsymbol{\xi})$. Hence, we get:

$$\begin{aligned}0 = \left|\boldsymbol{n}(\boldsymbol{\xi})^T\{\dot{\boldsymbol{\xi}}\}_t\right| &= \frac{1}{m}\int_0^T \left((1-w)\boldsymbol{n}^T\mathcal{D}^f\boldsymbol{n} + ws^o\right)\dot{\xi}\, dt \\ < \frac{1}{m}\int_0^T s^f\,\dot{\xi}\, dt &= \frac{s^f}{m}(\xi - \{\xi\}_0) + v^I\, dt\end{aligned} \qquad (32)$$

where $m = \max(\text{eig}(\mathcal{M}))$, with the maximum displacement as:

$$\|\{\xi\}_0 - \xi\| \leq \|v^I\|m/s^{\text{f}} \qquad (33)$$

Lemma IV.1 assumes constant velocity field $\boldsymbol{f}(\boldsymbol{\xi})$ and flat obstacle surface. This is an appropriate assumption for large velocities after disturbances towards the obstacle, i.e., $\|\boldsymbol{v}^I\| \gg \|\boldsymbol{f}(\boldsymbol{\xi})\|$ and starting close to the surface. Since the distance traveled has to be flat to avoid collision, the vectorfield is likely to show small changes, and the surface has little deviation.

Nevertheless, there is no guarantee against drifting into obstacles in the presence of highly curved surfaces and velocity fields. However, designing a repulsive field as proposed in [20] can ensure collision avoidance in such scenarios.

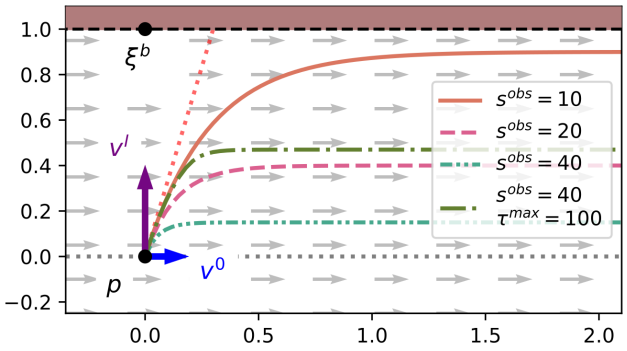

Fig. 5: A disturbance occurs of a point-agent at position $\boldsymbol{p}^0$ with velocity after the impact of $\{\dot{\boldsymbol{\xi}}\}_0 = \boldsymbol{v}^0 + \boldsymbol{v}^I$. A high damping in the direction of the obstacle in the presence of a constant velocity field (gray) ensures collision avoidance. Whereas different damping values s^{o} and optionally a maximum repulsion force $\boldsymbol{\tau}^{\max}$ lead to different trajectories.

V. Evaluation

The proposed obstacle aware controller[2] is compared to a baseline, the velocity preserving, passive controller [7].

A. Obstacle Aware Passivity Using a Robot Arm

The obstacle-aware passivity controller was implemented to guide a 7-degree-of-freedom robot arm (Panda from Franka Emika) while moving around a cubic obstacle.

The joint torque is computed using inverse kinematics combined with the proposed passive controller for the position, but a proportional controller for the orientation:

$$\boldsymbol{\tau}_q = \boldsymbol{J}^{\dagger}(\boldsymbol{q}) \begin{bmatrix} \mathcal{D}(\boldsymbol{\xi}) \left(\boldsymbol{f}(\boldsymbol{\xi}) - \dot{\boldsymbol{\xi}} \right) \\ p^{\alpha}(\boldsymbol{\alpha} - \boldsymbol{\alpha}^a) \end{bmatrix} \tag{34}$$

where $\boldsymbol{J}^{\dagger}$ represents the Moore-Penrose pseudo inverse of the Jacobian matrix, and $\boldsymbol{\alpha}$ and $\boldsymbol{\alpha}^a$ denote the end effector's orientation and the desired orientation, respectively. The angular damping parameter is chosen as $p^{\alpha} = 5.5$. The desired orientation $\boldsymbol{\alpha}^a$ is pointing downward with a quaternion value of $(w, x, y, z) = (0, 1, 0, 0)$. For the angle subtraction, we use quaternion representation to avoid singularities, but an angle-axis representation of the orientation is used to evaluate the torque from the angular offset.

The angular damping is chosen as $p^{\alpha} = 5.5$. The damping values are set as $s^{\mathrm{o}} = 160\,\mathrm{s}^{-1}$, $s^{\mathrm{f}} = 64\,\mathrm{s}^{-1}]$, and $s^{\mathrm{c}} = 16\,\mathrm{s}^{-1}$.

The robot start position is approximately at $\boldsymbol{\xi}_0 = [0.3\mathrm{m}, 0.4\mathrm{m}, 0.3\mathrm{m},]^T$ and the attractor is at position $\boldsymbol{\xi}^a = [0.26\mathrm{m}, -0.53\mathrm{m}, 0.33\mathrm{m}]^T$. The controller operates at a frequency of $500\,\mathrm{Hz}$. The robot encounters a single squared box with axes length $0.16\,\mathrm{m}$ and a margin of $0.12\,\mathrm{m}$, placed in front of the robot base (Fig. 6). The precise location of the box is tracked in real-time using a marker-based vision system (Optitrack). When passing the box, the robot is pushed with $\boldsymbol{t}^e$ towards the box. The experiment is

[2]Source code: `https://github.com/hubernikus/obstacle_aware_damping`

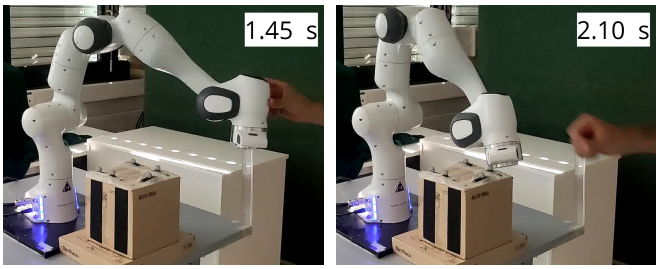

(a) Obstacle-aware controller rejects repulsion and avoids collision

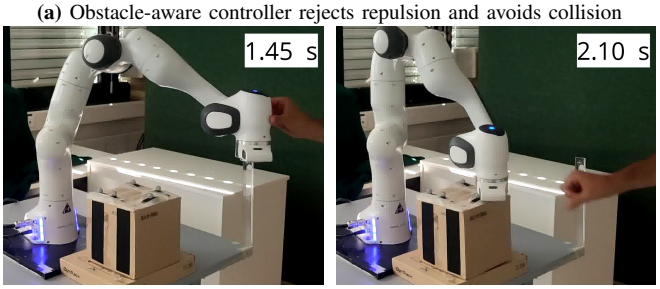

(b) Velocity preserving controller leads to collision with obstacle

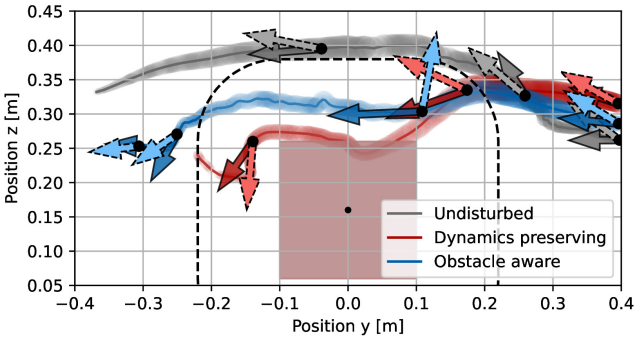

(c) The two control methods compared with the undisturbed trajectory. The wider line indicates a higher x-value. The darker arrow is the actual, and the desired velocity is the brighter arrow.

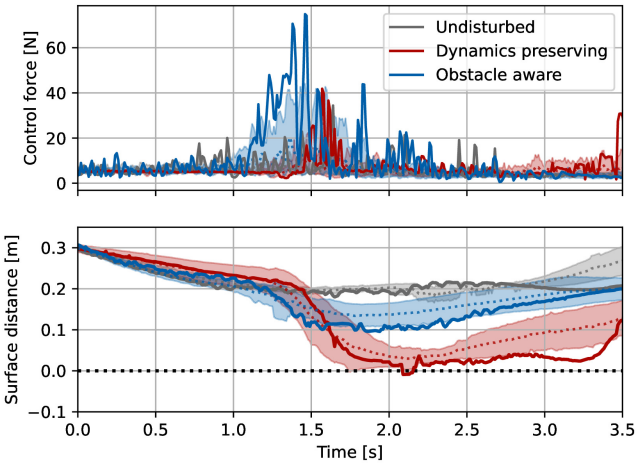

(d) The specific trajectory is represented by a full line, while the average (dashed line) and variance (shaded area) are evaluated over ten epochs. The mean and variance of the control force are evaluated in the logarithmic space.

Fig. 6: The robot arm, guided by the obstacle-aware passive controller, effectively avoids the disturbance towards the obstacle while maintaining a margin of $0.16\,\mathrm{m}$ around the obstacle. The experiment was repeated ten times with a similar disturbance applied to the robot arm in each run.

repeated ten times for both controllers and compared to the undisturbed motion.

This outcome is attributed to the obstacle-aware controller's stronger control force, with a high peak occurring around $1.45\,\mathrm{s}$ when the disturbance is encountered. In contrast, the velocity-preserving controller only acts when the robot almost collides, leading to a delayed response. Additionally, the obstacle-aware controller exhibits higher forces, contributing to improved tracking of the avoidance trajectory. These findings affirm the superior collision avoidance capabilities and tracking performance of the obstacle-aware passivity controller in real-world robot arm scenarios.

VI. Discussion

We introduced a novel passive obstacle-aware controller that takes as an input the desired, collision-free velocity and outputs a control torque. The stability proof enables the controller to be used with any bounded input velocity field, and this result extends to a general class of damping controllers. Furthermore, the controller is shown to reject disturbances, and the parameter-tuning for the discrete-time system has been analyzed. The controller was experimentally evaluated and compared to a baseline passive controller. Applied to a real robot arm, the disturbance force was successfully rejected, ensuring collision avoidance while following a reference motion.

A. Applicability and Theoretical Analysis

The theoretical analysis from Theorem III.1 indicates BIBO stability for a system with bounded desired velocity. Consequently, controllers like the damping-based approach in [7] do not require an energy tank. Yet, introducing an adaptive proportional term $\mathcal{K}$ can lead to instabilities [9], [10]. Careful consideration of the controller design and stability analysis is necessary to ensure robust and safe performance in practical applications. Nevertheless, the passivity proof enables a broad range of time-varying damping controllers to be safely applied to robotic systems.

B. Caution in Obstacle's Proximity

In this work, we assume the obstacles' position to be precisely known. However, in many scenarios, the robot might have limited perception as it approaches an obstacle. Hence, the robot should be more compliant to enable safe workspace exploration rather than increasing the damping. Future work should explore how to combine these two opposing paradigms: safe control for avoidance yet cautious exploration.

References

[1] L. Huber, A. Billard, and J.-J. Slotine, "Avoidance of convex and concave obstacles with convergence ensured through contraction," *IEEE Robotics and Automation Letters*, vol. 4, no. 2, pp. 1462–1469, 2019.

[2] N. Hogan, "Impedance control: An approach to manipulation: Part ii—implementation," 1985.

[3] B. Vanderborght, A. Albu-Schäffer, A. Bicchi, *et al.*, "Variable impedance actuators: A review," *Robotics and autonomous systems*, vol. 61, no. 12, pp. 1601–1614, 2013.

[4] F. J. Abu-Dakka and M. Saveriano, "Variable impedance control and learning—a review," *Frontiers in Robotics and AI*, vol. 7, p. 590 681, 2020.

[5] G. D. Glosser and W. S. Newman, "The implementation of a natural admittance controller on an industrial manipulator," in *Proceedings of the 1994 IEEE International Conference on Robotics and Automation*, IEEE, 1994, pp. 1209–1215.

[6] P. Y. Li and R. Horowitz, "Passive velocity field control of mechanical manipulators," *IEEE Transactions on robotics and automation*, vol. 15, no. 4, pp. 751–763, 1999.

[7] K. Kronander and A. Billard, "Passive interaction control with dynamical systems," *IEEE Robotics and Automation Letters*, vol. 1, no. 1, pp. 106–113, 2015.

[8] T. Fujiki and K. Tahara, "Series admittance–impedance controller for more robust and stable extension of force control," *ROBOMECH Journal*, vol. 9, no. 1, p. 23, 2022.

[9] F. Ferraguti, C. Secchi, and C. Fantuzzi, "A tank-based approach to impedance control with variable stiffness," in *2013 IEEE international conference on robotics and automation*, IEEE, 2013, pp. 4948–4953.

[10] K. Kronander and A. Billard, "Stability considerations for variable impedance control," *IEEE Transactions on Robotics*, vol. 32, no. 5, pp. 1298–1305, 2016.

[11] O. Khatib, "A unified approach for motion and force control of robot manipulators: The operational space formulation," *IEEE Journal on Robotics and Automation*, vol. 3, no. 1, pp. 43–53, 1987.

[12] D. E. Koditschek and E. Rimon, "Robot navigation functions on manifolds with boundary," *Advances in applied mathematics*, vol. 11, no. 4, pp. 412–442, 1990.

[13] S. Loizou and E. Rimon, "Mobile robot navigation functions tuned by sensor readings in partially known environments," *IEEE Robotics and Automation Letters*, 2022.

[14] V. Duindam, S. Stramigioli, and J. M. Scherpen, "Passive compensation of nonlinear robot dynamics," *IEEE transactions on robotics and automation*, vol. 20, no. 3, pp. 480–488, 2004.

[15] L. Singh, H. Stephanou, and J. Wen, "Real-time robot motion control with circulatory fields," in *Proceedings of IEEE International Conference on Robotics and Automation*, IEEE, vol. 3, 1996, pp. 2737–2742.

[16] S. Haddadin, R. Belder, and A. Albu-Schäffer, "Dynamic motion planning for robots in partially unknown environments," *IFAC Proceedings Volumes*, vol. 44, no. 1, pp. 6842–6850, 2011.

[17] O. Brock and O. Khatib, "Elastic strips: A framework for motion generation in human environments," *The International Journal of Robotics Research*, vol. 21, no. 12, pp. 1031–1052, 2002.

[18] A. Tulbure and O. Khatib, "Closing the loop: Real-time perception and control for robust collision avoidance with occluded obstacles," in *2020 IEEE/RSJ International Conference on Intelligent Robots and Systems (IROS)*, IEEE, 2020, pp. 5700–5707.

[19] C. I. Connolly, "Harmonic functions and collision probabilities," *The International Journal of Robotics Research*, vol. 16, no. 4, pp. 497–507, 1997.

[20] L. Huber, J.-J. Slotine, and A. Billard, *Avoidance of concave obstacles through rotation of nonlinear dynamics*, 2023. arXiv: 2306.16160 [cs.RO].

[21] L. Huber, J.-J. Slotine, and A. Billard, "Avoiding dense and dynamic obstacles in enclosed spaces: Application to moving in crowds," *IEEE Transactions on Robotics*, vol. 38, no. 5, pp. 3113–3132, 2022.

[22] J.-M. Bony, "Principe du maximum, inégalité de harnack et unicité du probleme de cauchy pour les opérateurs elliptiques dégénérés," in *Annales de l'institut Fourier*, vol. 19, 1969, pp. 277–304.